# The grid-dose-spreading algorithm for dose distribution calculation in heavy charged particle radiotherapy

Nobuyuki Kanematsu* and Shunsuke Yonai
*Department of Accelerator and Medical Physics, Research Center for Charged Particle Therapy, National Institute of Radiological Sciences, 4-9-1 Anagawa, Inage-ku, Chiba 263-8555, Japan*

Azusa Ishizaki
*Department of Quantum Science and Energy Engineering, Tohoku University, Aramaki-Aza-Aoba 01, Aoba-ku, Sendai 980-8579, Japan*
(Dated: December 14, 2007)

A new variant of the pencil-beam (PB) algorithm for dose distribution calculation for radiotherapy with protons and heavier ions, the grid-dose spreading (GDS) algorithm, is proposed. The GDS algorithm is intrinsically faster than conventional PB algorithms due to approximations in convolution integral, where physical calculations are decoupled from simple grid-to-grid energy transfer. It was effortlessly implemented to a carbon-ion radiotherapy treatment planning system to enable realistic beam blurring in the field, which was absent with the broad-beam (BB) algorithm. For a typical prostate treatment, the slowing factor of the GDS algorithm relative to the BB algorithm was 1.4, which is a great improvement over the conventional PB algorithms with a typical slowing factor of several tens. The GDS algorithm is mathematically equivalent to the PB algorithm for horizontal and vertical coplanar beams commonly used in carbon-ion radiotherapy while dose deformation within the size of the pristine spread occurs for angled beams, which was within 3 mm for a single 150-MeV proton pencil beam of 30° incidence, and needs to be assessed against the clinical requirements and tolerances in practical situations.

## I. INTRODUCTION

Ceaseless efforts for accuracy improvement and constant progress in computing technology have made the pencil-beam (PB) algorithm be the standard method for dose distribution calculation in heavy charged particle radiotherapy with protons and heavier ions.[1–11] In the PB algorithm, a treatment beam is divided into elementary pencil beams with developing transverse spread as they penetrate through heterogeneous medium to handle spatial modulation of beam scatter that is ignored in the broad-beam (BB) algorithm.[1,2] The dose distribution will be formed with superposition of the pencil beams using kernel-convolution techniques with variations in algorithmic implementation, for example, in choice of the coordinate system, order of the multiple integrals, and numerical approximations, which greatly influence the accuracy, speed, complexity, and generality of the code.[12,13]

Though the PB algorithm may be sufficiently accurate and fast for dose calculation in treatment planning in the present form, demand for faster calculation methods may always remain, for example, for optimization in the intensity-modulated radiotherapy with scanned charged particle beams,[10,14] and for adaptive radiotherapy under image guidance,[15,16] which will ultimately accommodate on-site re-planning for an immobilized patient quickly between imaging and treatment. Pursuing faster computational algorithms might be critical for the innovation to happen.

This paper presents one of such approaches, where we briefly review the BB and PB algorithms, describe the new algorithm, demonstrate the effectiveness in carbon-ion radiotherapy, evaluate the accuracy with a modeled proton pencil beam, and discuss the usefulness in heavy charged particle radiotherapy of the present and future.

## II. MATERIALS AND METHODS

### A. The broad-beam algorithm

In the BB algorithm, dose $D$ at point $\vec{r}$ is resolved into the BB dose and the penumbra effect.[1,2] The BB dose $D_{\mathrm{BB}}$, or equivalently dose per fluence of the incident beam, is given either theoretically or experimentally as a function of water-equivalent depth $w$ that is calculated with the ray-tracing integral of effective density $\rho$ from the beam source $\vec{r}_0$ in radial direction $\vec{v} = (\vec{r} - \vec{r}_0)/|\vec{r} - \vec{r}_0|$. The penumbra effect gradates the field edge with the error function $\mathrm{erf}(x) = (2/\sqrt{\pi}) \int_0^x \mathrm{e}^{-u^2} \mathrm{d}u$ of the signed closest distance to the geometrical field edge, $t$ ($t > 0$ for $\vec{r}$ in the field, $t < 0$ otherwise),

$$D(\vec{r}) = D_{\mathrm{BB}}\left(w(\vec{r})\right) \frac{1}{2} \left[1 + \mathrm{erf}\left(\frac{t\,(\vec{r})}{\sqrt{2}\,\sigma_{\mathrm{t}}(\vec{r})}\right)\right] \quad (1)$$

$$w(\vec{r}) = \int_0^{|\vec{r}-\vec{r}_0|} \rho\left(\vec{r}_0 + s\,\vec{v}(\vec{r})\right) \mathrm{d}s \quad (2)$$

where the projected transverse spread $\sigma_{\mathrm{t}}(\vec{r})$ is given either experimentally or theoretically.

The formulation of the penumbra effect simulates the dose-collecting process at point $\vec{r}$ from uniformly and continuously distributed invariant Gaussian sub-beams in the field. The assumed uniformity and invariance of the sub-beams restrict the validity of the model to a nar-

row penumbra region where the local-homogeneity approximation may be valid.

### B. The pencil-beam algorithm

In convolution algorithms, a dose distribution is generally calculated by kernel integral,

$$D(\vec{r}) = \int T(\vec{p})\, h(\vec{p},\vec{r})\, \mathrm{d}^3\vec{p}, \tag{3}$$

where $T(\vec{p})$ is the total energy released per mass (terma) from the radiation at point $\vec{p}$ and kernel function $h(\vec{p},\vec{r})$ is the terma fraction transfered to point $\vec{r}$.[13] In the PB algorithm, the terma equals the BB dose in the beam field or zero otherwise and is transversely spread by a planar Gaussian kernel,

$$T(\vec{p}) \;=\; \begin{cases} D_{\mathrm{BB}}\left(w(\vec{p})\right) & (\vec{p}\in \text{field}) \\ 0 & (\vec{p}\notin \text{field}) \end{cases} \tag{4}$$

$$h(\vec{p},\vec{r}) \;=\; \frac{1}{2\,\pi\,\sigma_{\mathrm{t}}^2(\vec{p})}\, \mathrm{e}^{-\frac{|\vec{r}-\vec{p}|^2}{2\,\sigma_{\mathrm{t}}^2(\vec{p})}}\, \delta\left((\vec{r}-\vec{p})\cdot\vec{v}(\vec{p})\right), \tag{5}$$

where the Dirac $\delta$ function restricts the spreading in the plane perpendicular to the PB direction $\vec{v}$, leading the convolution to an areal integral of a pencil kernel in the field.[1,2] In the numerical integration, several tens or more terma-emitting points are usually arranged around each of the dose-collecting points on the transverse plane with radial distance limitation $|\vec{r}-\vec{p}| < \alpha\sqrt{2}\,\sigma_{\mathrm{t}}$, where the Gaussian tail-cutoff parameter $\alpha$ is normally set to 3 and a normalization factor is multiplied to the kernel to compensate the ignored tail contributions.[2]

The PB algorithm accommodates the density heterogeneity by involving the ray-tracing integral Eq. (2) to derive the terma and the kernel within the convolution integral Eq. (3). The multiple integration will, however, increase the computational amount severely.

### C. The grid-dose-spreading algorithm

In treatment planning, the dose grids must be fine enough to show dose variation in the patient with grid spacing as small as $\sigma_{\mathrm{t}}$ or less and should be also able to represent distributions of any quantities. In the grid-dose-spreading (GDS) algorithm, the termas and the spreads in Eqs. (4) and (5) are calculated at all the dose grids and stored in three-dimensional arrays,

$$T_i \;=\; T(\vec{r}_i) \tag{6}$$

$$\sigma_{\mathrm{t}i} \;=\; \sigma_{\mathrm{t}}(\vec{r}_i), \tag{7}$$

for grid $i$ located at $\vec{r}_i = (x_i, y_i, z_i)$ in the grid-based coordinate system. The number of the ray-tracing integrals is minimized by extracting out of the convolution integral.

The gridded distributions, however, are not directly applicable to the convolution due to the coplanar constraint between terma emission and dose collection in the PB model because the PB axis is generally angled to the $x$, $y$, and $z$ grid axes with direction cosine vector $\vec{v} = (v_{\mathrm{x}}, v_{\mathrm{y}}, v_{\mathrm{z}})$. In order to resolve this difficulty, the disk-shaped kernel in Eq. (5) is deformed to the best approximate ellipsoidal kernel of the product of three Gaussian functions,

$$h(\vec{p},\vec{r}) \;\rightarrow\; \frac{\mathrm{e}^{-\frac{q_{\mathrm{x}}^2}{2\,\sigma_{\mathrm{x}}^2}}}{\sqrt{2\,\pi}\,\sigma_{\mathrm{x}}}\, \frac{\mathrm{e}^{-\frac{q_{\mathrm{y}}^2}{2\,\sigma_{\mathrm{y}}^2}}}{\sqrt{2\,\pi}\,\sigma_{\mathrm{y}}}\, \frac{\mathrm{e}^{-\frac{q_{\mathrm{z}}^2}{2\,\sigma_{\mathrm{z}}^2}}}{\sqrt{2\,\pi}\,\sigma_{\mathrm{z}}}, \tag{8}$$

where $\vec{q} = \vec{r}-\vec{p} = (q_{\mathrm{x}}, q_{\mathrm{y}}, q_{\mathrm{z}})$ is the displacement vector from the terma-emitting to dose-collecting points and $\sigma_{\mathrm{x}}$, $\sigma_{\mathrm{y}}$, and $\sigma_{\mathrm{z}}$ are the grid-axial projections of the spread,

$$\begin{aligned} \sigma_k^2(\vec{p}) \;&=\; \int q_k^2\, h(\vec{p},\vec{p}+\vec{q})\, \mathrm{d}^3\vec{q} \\ &=\; \left(1-v_k^2(\vec{p})\right)\, \sigma_{\mathrm{t}}^2(\vec{p}) \quad (k=\mathrm{x},\,\mathrm{y},\,\mathrm{z}), \end{aligned} \tag{9}$$

derived with the planar point kernel in Eq. (5). Applying the gridded distributions, the convolution in the PB algorithm in Eq. (3) is rewritten to

$$D_j = \sum_{i\in\left(|q_{k\,ij}|\le\alpha\,\sigma_k+\frac{\delta_k}{2}\right)_{\forall k}} T_i \prod_k \frac{h_{ki}(q_{k\,ij})}{\epsilon_{ki}} \tag{10}$$

where $D_j$ is the dose collected at grid $j$, $\vec{q}_{ij}$ is the displacement between grids $i$ and $j$, grid-axial spreading function $h_{ki}(q_{k\,ij})$ is the dose fraction transfered into width $\delta_k$ at grid $j$, and dose-collection acceptance $\epsilon_{ki}$ compensates the ignored Gaussian tails by cutoff parameter $\alpha$ for the summation. The grid-axial spreading functions and the acceptances are analytically given by

$$\begin{aligned} h_{ki}(q) \;&=\; \frac{1}{\sqrt{2\,\pi}\,\sigma_{ki}} \int_{q-\frac{\delta_k}{2}}^{q+\frac{\delta_k}{2}} \mathrm{e}^{-\frac{u^2}{2\,\sigma_{ki}^2}}\, \mathrm{d}u \\ &=\; \frac{1}{2}\left[\mathrm{erf}\left(\frac{|q|+\frac{\delta_k}{2}}{\sqrt{2}\,\sigma_{ki}}\right) - \mathrm{erf}\left(\frac{|q|-\frac{\delta_k}{2}}{\sqrt{2}\,\sigma_{ki}}\right)\right] \end{aligned} \tag{11}$$

$$\begin{aligned} \epsilon_{ki} \;&=\; \frac{1}{\sqrt{2\,\pi}\,\sigma_{ki}} \int_{-\alpha\,\sigma_{k\,i}-\frac{\delta_k}{2}}^{\alpha\,\sigma_{k\,i}+\frac{\delta_k}{2}} \mathrm{e}^{-\frac{u^2}{2\,\sigma_{ki}^2}}\, \mathrm{d}u \\ &=\; \mathrm{erf}\left(\frac{\alpha\,\sigma_{ki}+\frac{\delta_k}{2}}{\sqrt{2}\,\sigma_{ki}}\right), \end{aligned} \tag{12}$$

which can be quickly computed with the standard math library.

Since the effective kernel volume is conserved in the deformation, the computational amount is proportional to the cutoff cross section of the pencil beam or roughly to $\alpha^2$. The computational efficiency is maximized by adopting the convolution scheme so-called "the interaction point of view".[12] In this case, the acceptance-corrected terma $T_i/(\epsilon_{\mathrm{x}i}\,\epsilon_{\mathrm{y}\,i}\,\epsilon_{\mathrm{z}i})$ is calculated at each emitter grid $i$

and then is distributed with the fractions $\prod_k h_{ki}(q_{kij})$'s to the nearby grids $j$'s. The gridded dose distribution $D_j$ will be formed when all the terma emissions have been processed as above.

It is noted that the GDS and PB algorithms may share all the physical and computational models and their inaccuracies except for the grid quantization and the kernel deformation. In cases where these additional inaccuracies are substantially smaller than the other ones, the GDS and PB algorithms will be practically equivalent.

### D. Implementation to treatment planning system for carbon-ion radiotherapy

Carbon-ion radiotherapy has been practiced at National Institute of Radiological Sciences since 1994 with accelerator complex HIMAC,[17] and original treatment planning system HIPLAN,[18,19] where the BB algorithm has been consistently used to avoid disturbance to the ongoing clinical studies even though Petti and Kohno *et al.* explicitly showed that the BB algorithm involves principled inaccuracy due to lack of beam blurring in the field.[1,20]

The GDS algorithm as described in Sec. II C was implemented to HIPLAN using the existing framework of the BB code. The terma distribution $T(\vec{r})$ is calculated by applying $\sigma_{\rm t} \to 0$ in Eq. (1), where the depth–dose curve $D_{\rm BB}(w)$ is from the beam data library of HIPLAN,[21] for the range-modulated carbon-ion beams including relative biological effectiveness (RBE) correction.[17] Invariant $\sigma_{\rm t} = 4$ mm and $\alpha = 3$ are used to preserve the penumbra behavior of the BB algorithm for the 400-MeV/nucleon beams with the multileaf collimator.

Generally, two algorithms can be impartially compared only under exactly the same condition except for the essential algorithmic differences in implementation. In this regard, we can accurately compare the GDS and BB algorithms by applying them to the identical plan on the single HIPLAN system.

### E. Analytic proton pencil-beam model

Since the GDS algorithm is a variant of the PB algorithms with additional approximations, it is necessary and sufficient for the accuracy evaluation to examine how the GDS calculation reproduces a modeled pencil beam under realistic conditions in grid spacing, transverse spread, and incident angle. For this purpose, we take a proton beam in water, or the proton pencil kernel itself, because the simplicity and the largest spread among the ion species will clarify the algorithmic error. Bortfeld established an analytic formula for the proton Bragg curve in water,[22] $D_{\rm BB}(w)$ in our notation, and Hong *et al.* tabulated the projected transverse scatter of protons in water,[2] $\sigma_{\rm t}(w)$, which determine the analytic PB model in Eqs. (3), (4), and (5) for reference.

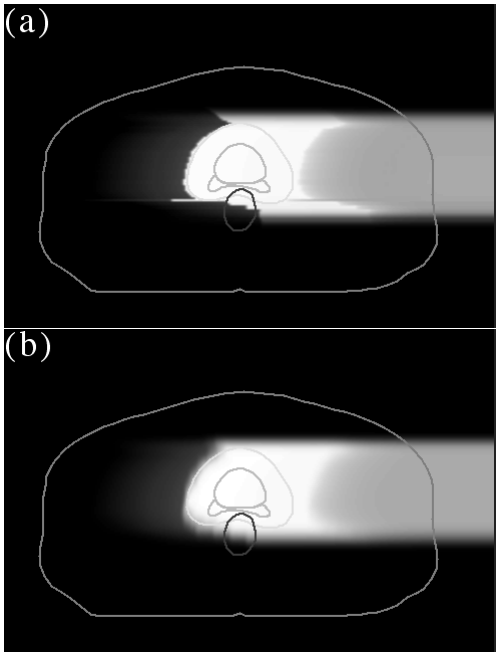


FIG. 1: Clinical dose distributions in a transaxial plane (43 cm × 28 cm) from a carbon-ion beam for prostate treatment calculated with the (a) BB and (b) GDS algorithms, where a prostate and seminal vesicles (gray lines) are included in the target (light gray) that partly overlaps with a rectum (dark gray) in a patient (gray), a horizontal beam is incident from the patient's left (the figure's right), and the doses are in linear gray scale (black for zero to white for the maximum).

In applying the GDS algorithm to this system, since Eq. (4) is not applicable to the infinitesimal field, the gridded terma and spread distributions are calculated according to the definition as total energy released per mass and the dose-weighted avarage in the grid-$i$ voxel ,

$$T_i = \frac{1}{V_0} \int_{s_{{\rm in}\,i}}^{s_{{\rm out}\,i}} D_{\rm BB}\left(w(s)\right)\,{\rm d}s \tag{13}$$

$$\sigma_{{\rm t}i}^2 = \frac{1}{V_0\,T_i} \int_{s_{{\rm in}\,i}}^{s_{{\rm out}\,i}} \sigma_{\rm t}^2\left(w(s)\right)\,D_{\rm BB}\left(w(s)\right)\,{\rm d}s, \tag{14}$$

where $V_0$ is the volume of the voxel, and $s_{{\rm in}\,i}$ and $s_{{\rm out}\,i}$ are the distances on the beam axis to enter and to exit from the voxel, respectively. The subsequent formulation for convolution in Sec. II C is applicable to this system.

For a broad-beam system, the terma and spread distributions are formed with summation and terma-weighted averaging of those of the pencil beams in Eqs. (13) and (14), respectively, and then a single volumetric convolution is quickly applied to form a dose distribution.

## III. RESULTS

### A. Performance in carbon-ion radiotherapy

Figure 1 shows the clinical, or RBE-weighted, dose distributions of the GDS and BB calculations on HIPLAN for a clinical case of carbon-ion radiotherapy for prostate. The clinical target volume (CTV) consisting of the prostate and the seminal vesicles, the rectum as an organ at risk, and the planning target volume (PTV) with 5-mm margin to the rectum side and 10-mm margin elsewhere added to the CTV, were manually segmented.[23] The effective density distribution for heterogeneity correction was derived from the planning CT image,[24] with grid spacings of 1.758 mm along the right–left and anterior–posterior axes and 2.500 mm along the inferior–superior axis, which are shared by the dose distributions.

A horizontal beam was conformed to the PTV with minimum 6 mm field margin using a multileaf collimator and was customized with a range compensator, a sculptured plastic object attached to the port, to absorb extra penetration of the carbon ions beyond the PTV with 3 mm depth margin. The compensator was designed in the $3 \times 3$ mm$^2$-sized pixel-array format with steepness limited by the maximum depth step of 15 mm considering the tapered structure of the milling tool. In this example, the rectum side of the PTV is almost parallel to the horizontal beam and the range compensation results in steep variation in beam range or so-called range discontinuity.

The BB calculation in Fig. 1(a) exhibits unphysically too sharp dose gradient at the range discontinuity around the rectum at risk, which could be influential on the clinical plan review. The ripples and the spikes of the range surface came from incomplete range compensation within the $3\times3$-mm$^2$ pixels. These artifacts have been naturally smeared out in the GDS calculation in Fig. 1(b).

While the BB algorithm was designed to reproduce the error function of $\sigma_{\rm t} = 4$ mm in the penumbra region, there was submillimeter-level disagreement between the BB and GDS calculations in field edge defined by 50%-dose position, which is consistent with the grid-quantization error of the GDS algorithm. The BB and GDS calculations for the prostate treatment case took 48 s and 66 s with SGI® Octane workstation, respectively. Namely, the GDS calculation was 1.4 times slower than the BB calculation in this case.

### B. Performance for angled proton pencil beam

Figure 2 shows dose distributions in water projected onto the $x$–$z$ plane, where a point-like 150-MeV proton beam with projected angular spread $\theta_0 = 10$ mrad is generated at 10 cm above water level with zenith angle 30°, namely with $\vec{r}_0 = (10/\sqrt{3}, 0, 10)$ cm and $\vec{v} = (-1/2, 0, -\sqrt{3}/2)$ in the grid-based coordinate system with origin defined at the beam entrance point into water. The divergent term $\theta_0\, s$ is quadratically added to the tabulated in-water spread,[2] in $\sigma_{\rm t}(\vec{r})$. The grid spacings in the GDS calculation are all 2 mm along the three axes.

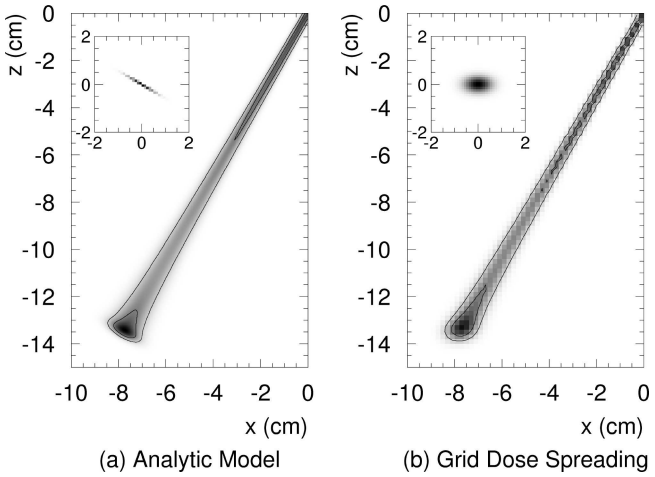


FIG. 2: Dose distributions from a proton pencil beam in water projected onto the $x$–$z$ plane, (a) the analytic beam model and (b) the corresponding GDS calculation. The $z$ axis is the vertical height from the water level and the $x$ axis is the relative horizontal position. The 20% and 50% isodose lines relative to the analytic maximum of 29.2 MeV g$^{-1}$ cm per incident proton are drawn with the gray scale images. The embedded images show the point-spread functions.

At relatively shallow depth, the GDS and the analytic model calculations are consistent within the grid resolution especially in the 20% isodose line while the 50% isodose line suffers from small dose errors under the low-dose-gradient condition. At the Bragg peak, there is substantial disagreement in the 20% isodose line within 3 mm.

The embedded images in Fig. 2 show the point-spreading functions with projected transverse spread of $\sigma_{\rm t} = 4.5$ mm at the Bragg peak, where the spreading in the analytic model is confined in the transverse plane and that in the GDS algorithm forms an ellipsoidal volume. In other words, the planar spreading is approximately resolved into the three uncorrelated orthogonal spreading by $\sigma_{\rm x} = 3.9$ mm, $\sigma_{\rm y} = 4.5$ mm, and $\sigma_{\rm z} = 2.3$ mm, which has deformed the point-spreading function, or the point kernel, and consequently the dose distribution.

Though both of the GDS and analytic-PB calculations were instantaneous with the single pencil beam, the PB calculation would slow down proportionally with the number of pencil beams for convolution. In fact, Hong *et al.* studied the BB and PB algorithms for proton radiotherapy and found that the PB calculation was slower than the BB calculation by factor of 73.[2]

## IV. DISCUSSION

In the GDS algorithm, the terma distribution is calculated as an intermediate quantity with grid quantiza-

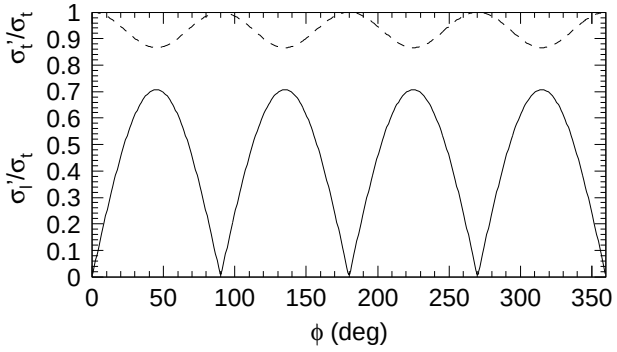


FIG. 3: The longitudinal ($\sigma_{\rm l}'$; solid line) and transverse ($\sigma_{\rm t}'$; dashed line) spreads of a coplanar beam reprojected from the deformed kernel in the GDS algorithm relative to the original transverse spread ($\sigma_{\rm t}$) as a function of gantry angle ($\phi$).

tion errors, which will propagate to the dose distribution. However, the quantization error will be usually negligible with sufficiently fine grid spacing. For example, in the prostate treatment case with grid spacing of 1.758 mm, the rms error from the quantization will be as small as $1.758/\sqrt{12} \approx 0.5$ mm, which is by far better than the realistic accuracy in target delineation.

The kernel deformation observed in the proton pencil beam case will greatly depend on beam direction with respect to the grid axes. When the beam is angled to all the three grid axes, the transverse planar spreading is approximated by volumetric spreading that includes an artifactual longitudinal component. The longitudinal spread $\sigma_{\rm l}'$ and the transverse spread $\sigma_{\rm t}'$ of the deformed kernel are derived from reprojection and conservation of the spread squared,

$$\sigma_{\rm l}' = \sqrt{\sum_k \sigma_k^2\, v_k^2} = \sqrt{1 - v_{\rm x}^4 - v_{\rm y}^4 - v_{\rm z}^4}\,\sigma_{\rm t} \qquad (15)$$

$$\sigma_{\rm t}' = \sqrt{\sigma_{\rm t}^2 - \frac{\sigma_{\rm l}'^2}{2}} = \frac{1}{\sqrt{2}}\sqrt{1 + v_{\rm x}^4 + v_{\rm y}^4 + v_{\rm z}^4}\,\sigma_{\rm t}, \qquad (16)$$

which are a measure of inaccuracy in distal fall off and a measure of accuracy in lateral penumbra, respectively, and will be both $\sqrt{(2/3)}\,\sigma_{\rm t}$ in the worst case with direction $\vec{v} = (\pm 1, \pm 1, \pm 1)/\sqrt{3}$. Figure 3 shows the reprojected spreads as a function of gantry angle $\phi$ in coplanar beam arrangement with $v_{\rm y} \approx 0$, which explains the deformation of the proton pencil beam at $\phi = 30^\circ$ in Sec. III B. In general, inaccuracy will have to be assessed against the clinical tolerances in realistic situations.

The spread of a pristine pencil beam limits the granularity of the dose distribution and may naturally approximate the necessary and sufficient spatial resolution for beam control and dose evaluation. The finer structure below the resolution and the various spatial uncertainties are normally tolerated with appropriate margins. In fact, the PTV should include substantial margins against patient setup error and internal organ motion of typically a few to several millimeters,[25] for example 5 to 10 mm for the prostate in Sec. III A. For clinical proton beams, the 20%–80% penumbra size may grow as large as 10 mm,[2] or $\sigma_{\rm t} \approx 10/1.68 \approx 6$ mm, against which, a field margin of $1.5\,\sigma_{\rm t} \sim 2\,\sigma_{\rm t} \approx 10$ mm around the PTV is usually added. Then, even with the worst direction $\vec{v} = (\pm 1, \pm 1, \pm 1)/\sqrt{3}$, the artifact as large as $\sigma_{\rm l}' = \sqrt{(2/3)}\,\sigma_{\rm t} \approx 5$ mm will be mostly covered up by those margins.

Generally for broad beams, the systematic deformation of the kernels uniformly distributed in the field will be mostly compensated except for field edges in analogy to the kernel-tilting approximation for photon beams.[26] The spread and hence the deformation will be even smaller with heavier-ion beams. In addition, when a vertical or horizontal coplanar beam is used in conjunction with planning CT in treatment position, namely with $\phi = 0$ or 90 in Fig. 3, the artifact will be completely absent, which has been almost always the case in carbon-ion radiotherapy with HIMAC and will be as well with its planned successors.[27] The GDS algorithm is in principle applicable to scanned beams. However, application to multidirectional intensity-modulated beams,[10,14] requires some caution because the kernel deformation will not be compensated even in the middle of the treated volume.

## V. CONCLUSIONS

A new variant of the PB algorithm, the GDS algorithm, is proposed for heavy charged particle radiotherapy with approximations of the gridded intermediate distributions and a modified convolution kernel for grid-to-grid energy transfer. The resultant high-speed nature and easiness of implementation are distinctive features of the GDS algorithm.

When the beam incidence is angled to all the dose-grid axes, the approximation will cause deformation in dose distribution within the size of the pristine spread at field edges. Such inaccuracy will have to be assessed relatively against the clinical tolerances and the other sources of errors in practical situations.

* Electronic address: nkanemat@nirs.go.jp

[1] P. L. Petti, "Differential-pencil-beam dose calculations for charged particles," Med. Phys. **19**, 137–149 (1992).

[2] L. Hong, M. Goitein, M. Bucciolini, R. Comiskey, B. Gottschalk, S. Rosenthal, C. Serago, and M. Urie, "A pencil beam algorithm for proton dose calculations," Phys. Med. Biol. **41**, 1305–1330 (1996).

[3] J. O. Deasy, "A proton dose calculation algorithm for con-

formal therapy simulations based on Molière's theory of lateral deflections" Med. Phys. **25**, 476–483 (1998).

[4] N. Kanematsu, T. Akagi, Y. Futami, A. Higashi, T. Kanai, N. Matsufuji, H. Tomura, and H. Yamashita, "A proton dose calculation code for treatment planning based on the pencil beam algorithm," Jpn. J. Med. Phys. **18**, 88–103 (1998).

[5] B. Schaffner, E. Pedroni, and A. Lomax, "Dose calculation models for proton treatment planning using a dynamic beam delivery system: an attempt to include density heterogeneity effects in the analytical dose calculation," Phys. Med. Biol. **44**, 27–41 (1999).

[6] K. R. Russell, U. Isacsson, M. Saxner, A. Ahnesjö, E. Montelius, E. Grusell, C. Vallhagen Dahlgren, S. Lorin, and B. Glimelius, "Implementation of pencil kernel and depth penetration algorithms for treatment planning of proton beams," Phys. Med. Biol. **45** 9–27 (2000).

[7] M. Krämer, O. Jäkel, T. Haberer, D. Schardt, and U. Weber, "Treatment planning for heavy-ion radiotherapy: physical beam model and dose optimization," Phys. Med. Biol. **45**, 3299–3317 (2000).

[8] H. Szymanowski, A. Mazal, C. Nauraye, S.Biensan, M. C. Murillo, S. Caneva, G. Gaboriaud, and J. C. Rosenwald, "Experimental determination and verification of the parameters used in a proton pencil beam algorithm," Med. Phys. **28**, 975–987 (2001).

[9] M. Hollmark, J. Uhrdin, D. Belkić, I. Gudowska, and A. Brahme, "Influence of multiple scattering and energy loss straggling on the absorbed dose distributions of therapeutic light ion beams: I. Analytical pencil beam model," Phys. Med. Biol. **49**, 3247–3265 (2004).

[10] M. Soukup, M. Fippel, and M. Alber, "A pencil beam algorithm for intensity modulated proton therapy derived from Monte Carlo simulations," Phys. Med. Biol. **50**, 5089–5104 (2005).

[11] N. Kanematsu, T. Akagi, Y. Takatani, S. Yonai, H. Sakamoto, and H. Yamashita, "Extended collimator model for pencil-beam dose calculation in proton radiotherapy," Phys. Med. Biol. **51**, 4807–4817 (2006).

[12] T. R. Mackie, J. W. Scrimger, and J. J. Battista, "A convolution method of calculating dose for 15-MV x rays," Med. Phys. **12**, 188–196 (1985)

[13] A. Ahnesjö and M. M. Asparadakis, "Dose calculations for external photon beams in radiotherapy," Phys. Med. Biol. **44**, R99–R155 (1999).

[14] A. Lomax, T. Boehringer, A. Coray, G. Goitein, M. Goitein, M. Grossmann, P. Juelke, S. Lin, E. Pedroni, B. Roher, W. Roser, B. Rossi, B. Siegenthaler, O. Stadelmann, H. Stauble, C. Vetter, and L. Wisser, "Intensity modulated proton therapy: A clinical example," Med. Phys. **28**, 317–324 (2001).

[15] D. Yan, F. Vicini, J. Wong, and A. Martinez, "Adaptive radiation therapy," Phys. Med. Biol. **42**, 123–132 (1997).

[16] T. R. Mackie, "Image guidance for precise conformal radiotherapy," Int. J. Radiat. Oncol. Biol. Phys. **56**, 89–105 (2003).

[17] T. Kanai, M. Endo, S. Minohara, N. Miyahara, H. Koyama-Ito, H. Tomura, N. Matsufuji, Y. Futami, A. Fukumura, T. Hiraoka, Y. Furusawa, K. Ando, M. Suzuki, F. Soga, and K. Kawachi, "Biophysical characteristics of HIMAC clinical irradiation system for heavy-ion radiation therapy," Int. J. Radiat. Oncol. Biol. Phys. **44**, 201–210 (1999).

[18] M. Endo, H. Koyama-Ito, S. Minohara, H. Tomura, T. Kanai, K. Kawachi, H. Tsujii, and K. Morita, "HIPLAN—A heavy ion treatment planning system at HIMAC," J. Jpn. Soc. Ther. Radiol. Oncol. **8**, 231–238 (1996).

[19] N. Kanematsu, M. Endo, Y. Futami, T. Kanai, H. Asakura, H. Oka, and K. Yusa, "Treatment planning for the layer-stacking irradiation system for three-dimensional conformal heavy-ion radiotherapy," Med. Phys. **29**, 2823–2829 (2002).

[20] R. Kohno, N. Kanematsu, T. Kanai, and K. Yusa, "Evaluation of a pencil beam algorithm for therapeutic carbon ion beam in presence of bolus," Med. Phys. **31**, 2249–2253 (2004).

[21] N. Kanematsu, M. Torikoshi, M. Mizota, and T. Kanai, "Secondary range shifting with range compensator for reduction of beam data library in heavy-ion radiotherapy," Med. Phys. **34**, 1907–1910 (2007).

[22] T. Bortfeld, "An analytical approximation of the Bragg curve for therapeutic proton beams," Med. Phys. **24**, 2024–2033 (1997).

[23] H. Tsuji, T. Yanagi, H. Ishikawa, T. Kamada, J. Mizoe, T. Kanai, S. Morita, and H. Tsujii, "Hypofractionated radiotherapy with carbon ion beams for prostate cancer," Int. J. Radiat. Oncol. Biol. Phys. **63**, 1153–1160 (2005).

[24] N. Kanematsu, N. Matsufuji, R. Kohno, S. Minohara, and T. Kanai, "A CT calibration method based on the polybinary tissue model for radiotherapy treatment planning," Phys. Med. Biol. **48**, 1053–1064 (2003).

[25] K. M. Langen and D. T. L. Jones, "Organ motion and its management,"Int. J. Radiat. Oncol. Biol. Phys. **50**, 265–278 (2001).

[26] M. B. Sharpe and J. J. Battista, "Dose calculations using convolution and superposition principles: the orientation of dose spread kernels in divergent x-ray beams," Med. Phys. **20**, 1685–1694 (1993).

[27] K. Noda, T. Furukawa, Y. Iwata, T. Kanai, M. Kanazawa, N. Kanematsu, A. Kitagawa, M. Komori, S. Minohara, T. Murakami, M. Muramatsu, S. Sato, Y. Sato, S. Shibuya, M. Torikoshi, and S. Yamada, "Design of carbon therapy facility based on 10 years experience at HIMAC," Nucl. Instrum. Methods Phys. Res. A **562**, 1038–1041 (2006).